APL Photonics

# Quantum communication with time-bin entanglement over a wavelength-multiplexed fiber network

Cite as: APL Photonics **7**, 016106 (2022); https://doi.org/10.1063/5.0073040
Submitted: 27 September 2021 • Accepted: 31 December 2021 • Accepted Manuscript Online: 31 December 2022 • Published Online: 25 January 2022

Jin-Hun Kim, Jin-Woo Chae, Youn-Chang Jeong, et al.

# Quantum communication with time-bin entanglement over a wavelength-multiplexed fiber network

Cite as: APL Photon. 7, 016106 (2022); doi: 10.1063/5.0073040
Submitted: 27 September 2021 • Accepted: 31 December 2021 •
Published Online: 25 January 2022



Jin-Hun Kim,[1] Jin-Woo Chae,[1] Youn-Chang Jeong,[2] and Yoon-Ho Kim[1,a)]

AFFILIATIONS

[1] Department of Physics, Pohang University of Science and Technology (POSTECH), Pohang 37673, South Korea
[2] The affiliated institute of ETRI, Daejeon 34044, South Korea

[a)] Author to whom correspondence should be addressed: yoonho72@gmail.com

## ABSTRACT

In a quantum network involving multiple communicating parties, an important goal is to establish high-quality pairwise entanglement among the users without introducing multiple entangled-photon sources which would necessarily complicate the overall network setup. Moreover, it is preferable that the pairwise entanglement of photons is in the time-bin degree of freedom as the photonic time-bin qubit is ideally suited for fiber-optic distribution. Here, we report an experimental demonstration of a field-deployable quantum communication network involving multiple users, all of whom share pairwise entanglement in the time-bin degree of freedom of photons. In particular, by utilizing a single spontaneous-parametric down-conversion source which produces a broadband pair of photons and the wavelength-division demultiplexing/multiplexing technology, all the communicating parties within the network are always simultaneously ready for quantum communication. To further demonstrate the practical feasibility of a quantum network with time-bin entanglement over a wavelength-multiplexed fiber network, we demonstrate entangled-photon quantum key distribution with three users, each separated by 60 km of optical fibers.



## I. INTRODUCTION

One of the principal goals in quantum communication is to distribute photonic entanglement to distant parties, thereby establishing a quantum channel, to enable implementations of certain entanglement-based communication protocols that are not possible classically, e.g., quantum teleportation,[1–5] quantum key distribution (QKD),[6–9] dense coding,[10–12] and quantum secret sharing.[13–15] In recent years, tremendous technical achievements toward long-distance quantum communication have been reported via free-space[16,17] and via optical fiber links.[18,19] Nevertheless, it remains to be a formidable problem to expand quantum communication to include multiple communicating parties, i.e., to build a quantum network, as it requires overcoming many fundamental and technical challenges. Given the importance of the quantum network in quantum information technology, a number of interesting ideas and technical achievements toward the quantum network have been reported, including the quantum repeater,[20–22] quantum memory,[23–27] generalized quantum measurement,[28–31] qudit entanglement,[32–35] hyper-entanglement,[36–39] trusted nodes,[40–43] active-switching,[44–47] wavelength-division multiplexing (WDM),[48–52] wavelength selective switch,[53–55] decoy state QKD,[56,57] and twin-field QKD.[58–61] While these developments certainly constitute important building blocks toward the global quantum network, a full-fledged quantum network is likely to be years away from fruition.

On the other hand, an elementary quantum network involving multiple communicating parties sharing bipartite entanglement is of practical significance as it can be used for certain important quantum communication tasks, such as teleportation and quantum key distribution. In this work, we report an experimental implementation of a field-deployable fiber-optic quantum communication network involving multiple users, all of whom share pairwise entanglement in the time-bin degree of freedom of photons. The fiber optic quantum network is based on a single entangled-photon source which distributes a pair of time-bin entangled qubits to any two members of the quantum network, and through the use of the wavelength-division demultiplexing/multiplexing technology, all the network members are simultaneously ready for quantum communication. The fact that each network member does not have to be equipped with its own entangled-photon source (only the network provider needs to be equipped with the entangled-photon source) greatly reduces the complexity and the cost of the network setup. Moreover, the network can be easily scaled up to include more users due to the use of the WDM technology without requiring trusted nodes or trusting the network provider. To further demonstrate the practical feasibility of a quantum network with entangled time-bin qubits over a wavelength-multiplexed fiber network, we demonstrate entangled-photon quantum key distribution with three users, each separated by 60 km of optical fibers.

## II. RESULTS AND DISCUSSION

### A. Experimental setup

The simplified experimental schematic of the quantum network, involving the network provider and three users, is shown in Fig. 1. The network provider consists of the source of entangled time-bin qubit pairs and the network nodes based on WDM technology. We first describe the source of entangled time-bin qubit pairs. A picosecond mode-locked fiber laser (FPL-02CTT, Calmar Laser) operating at the wavelength of 1552.52 nm (the FWHM bandwidth is 0.4 nm) and at the repetition rate of 18.02 MHz is frequency-doubled to 776.26 nm via the second harmonic generation (SHG) process at the type-0 bulk PPLN crystal (which is 35 mm long and has the polling period of 19.3 $\mu$m; HC Photonics). Before the SHG process, the laser pulse goes through an unbalanced Michelson

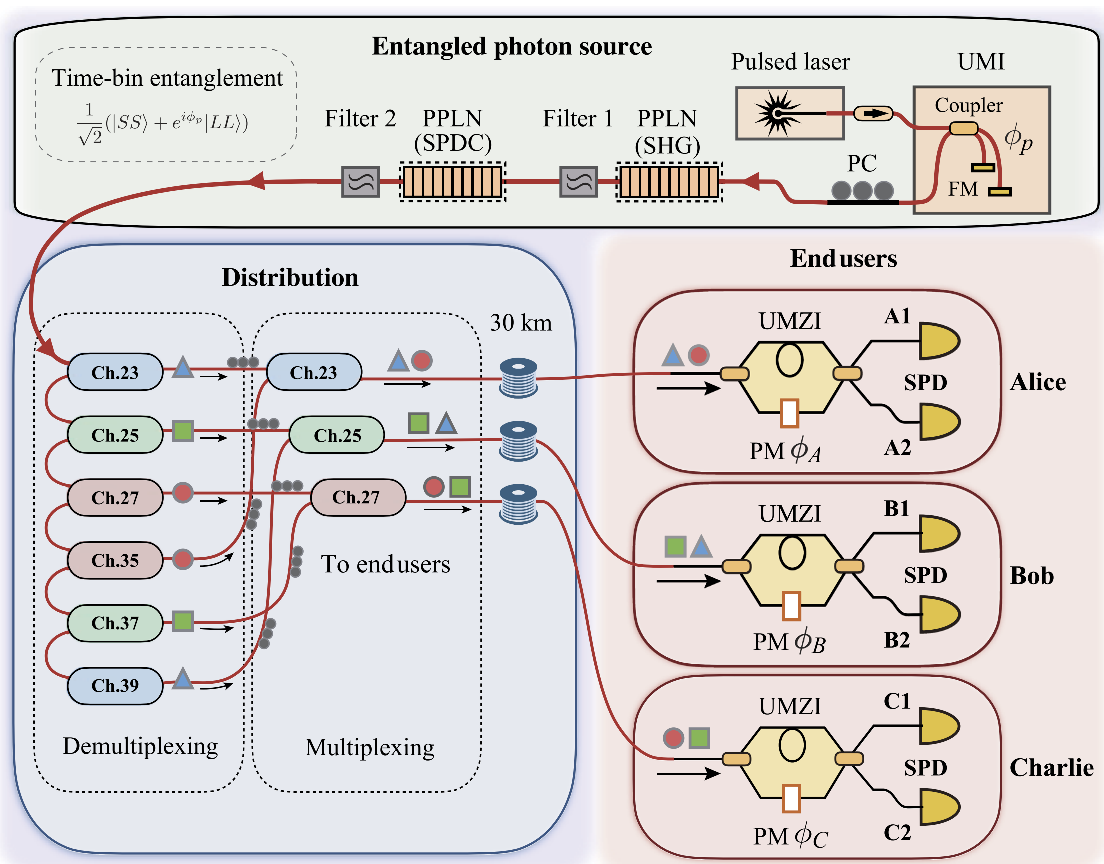


**FIG. 1.** Scheme for the multi-party quantum network in which every member shares entangled time-bin qubit pairs. The network provider consists of the source of entangled time-bin qubit pairs and the network nodes based on dense wavelength-division multiplexing (DWDM) technology. The channel numbers follow the DWDM ITU grid specification for the telecom C-band 100 GHz grid. The users (Alice, Bob, and Charlie) are connected to the nodes via 30 km optical fiber spools, and every user shares entangled time-bin qubit pairs. To establish the time-bin entanglement in the experiment, three frequency-correlated pairs, simultaneously present with time-bin entanglement, are utilized and distributed among three users so that each frequency pair could be shared by each user pair. The frequency pairs are symbolically represented by pairs of blue triangles, green squares, and red circles. All interferometers (an UMI and three UMZIs) are actively stabilized using auxiliary lasers and feedback control. UMI: unbalanced Michelson interferometer, FM: Faraday mirror, PC: polarization controller, PPLN: periodically poled lithium niobite, SHG: second harmonic generation, SPDC: spontaneous parametric down-conversion, UMZI: unbalanced Mach–Zehnder interferometer, and PM: phase modulator.

interferometer (UMI) to create a pair of pulses separated by 3.6 ns, which defines the time bins in our experiment. To prevent the thermal phase drift of the UMI, which consists of fiber-optic couplers, Faraday mirrors (FMs), a variable attenuator, a variable delay line, and a piezo-actuated fiber stretcher, an auxiliary CW laser of 1553.33 nm is used to actively stabilize the interferometer. The coherence length of the auxiliary CW laser is much larger than the path length difference of the UMI and the interference signal of the auxiliary CW laser is used to feedback-control the piezo-actuated fiber stretcher, thus stabilizing the interferometer. Note that the UMI auto-compensates for the polarization-mode dispersion due to the use of Faraday mirrors.

Spontaneous parametric down-conversion (SPDC) of the pump pulse pair of 776.26 nm at the type-0 waveguide PPLN (20 mm in length and has the poling period of 17.0 $\mu$m; HC Photonics) prepares the two-photon state of the form[62–64]

$$\frac{1}{\sqrt{2}}\Big(|S\rangle_s|S\rangle_i + e^{i\phi_p}|L\rangle_s|L\rangle_i\Big) \otimes \int d\omega_s d\omega_i f(\omega_s,\omega_i)|\omega_s,\omega_i\rangle, \qquad (1)$$

where $|S\rangle_s|S\rangle_i$ denotes the probability amplitude that the SPDC photon pair (often termed the signal and the idler, as identified by the subscript s and $i$) is created by the earlier pump pulse and $|L\rangle_s|L\rangle_i$ denotes the probability amplitude for the SPDC photon pair created by the latter pump pulse. The joint spectral intensity $|f(\omega_s,\omega_i)|^2$ defines the spectral correlation between the signal and the idler photons as well as the marginal spectral distribution of the individual SPDC photons. In the experiment, due to the use of type-0 PPLN for SPDC, the SPDC bandwidth is over 80 nm in the FWHM, centered at 1552.52 nm. The relative phase term $\phi_p$ may be controlled by fine-tuning the piezo-actuated fiber stretcher at the UMI. Any residual telecomband laser light behind the SHG module and near-IR pump light behind the SPDC module are suppressed by filter 1 and filter 2, respectively, which are composed of dichroic mirrors designed to reflect the unwanted light. They have the rejection ratio of 80 dB (at 1550 ± 30 nm for filter 1 and at 775 ± 30 nm for filter 2) and the insertion loss of 2.0 dB (at 775 ± 30 nm for filter 1 and at 1550 ± 30 nm for filter 2).

The distribution nodes of the time-bin entangled photon pair to the network users are made up with various WDM modules for demultiplexing (DEMUX) and multiplexing (MUX) correlated-frequency components of the time-bin entangled SPDC photon pairs to the network users (see Fig. 1). As seen in Eq. (1), the signal and idler photons of SPDC are frequency-time entangled (in addition to the time-bin entanglement), i.e., if the signal photon is measured to have the wavelength $\lambda_s$, the idler photon must have the wavelength $\lambda_i$ determined by the phase-matching condition. Since the spectral bandwidth of SPDC is roughly 80 nm in the FWHM with the flat-top region of the spectrum spanning ~40 nm (due to the use of type-0 SPDC), the frequency-correlated photon pairs can be selectively transmitted to any pair of the network users to establish an entangled quantum channel by using commercially available telecom C-band dense wavelength-division multiplexing (DWDM) components. First, DWDM demultiplexers are used to discretize the incoming entangled photons into several different spatial modes according to the correlated frequencies. In this work, we consider three end users, i.e., Alice, Bob, and Charlie, each sharing time-bin entanglement with each other, so six DWDM channels are utilized: DWDM channels 35, 37, and 39 are used for the signal photons and 23, 25, and 27 are used for the idler photons. The frequency-correlated DWDM channel pairs are $\{35, 27\}$, $\{37, 25\}$, and $\{39, 23\}$, and the channel numbers follow the DWDM ITU grid specification for the telecom C-band 100 GHz grid. The DWDM components in use have the 3 dB spectral bandwidth of 150 GHz. Then, to distribute time-bin entangled photon pairs to every user, two uncorrelated DWDM channels are multiplexed into a single fiber optic mode, resulting in three output nodes to which network users are connected. In this work, Alice, Bob, and Charlie are connected via 30 km long dispersion-shifted fiber spools (FSC-DSF-spool; Lucent), and therefore, time-bin entanglement is established between Alice–Bob, Bob–Charlie, and Alice–Charlie via 60 km long optical fibers. Note that the distribution nodes can be easily expanded to include more network users by using additional DWDM channels in the fashion described above. To prepare a fully connected network with $N$ users, we need to establish $N(N-1)/2$ links, so the total number of necessary DWDM channels is calculated to be $N(N-1)$. Considering the 40 nm flat-top spectral bandwidth of SPDC photons (our experimental condition), we estimate that roughly 11 network users can be accommodated easily in our setup if we exploit the 50-GHz grid DWDM channels. To add more users, even narrower-band DWDM channels and an SPDC source of broader bandwidth would be needed.

At the analysis and measurement stage, the end users are equipped with his/her own unbalanced Mach–Zehnder interferometers (UMZI) and InGaAs single-photon detectors (SPD-A-NIR; AUREA Technology), as shown in Fig. 1. The path length difference of the UMZI is set to the same as that of the UMI (i.e., the time-bin separation of 3.6 ns), and UMZIs include a fiber-optic phase modulator in the short arm and in the long arm a set of a variable delay line, a piezo-actuated fiber stretcher, and an electronically driven fiber polarization controller. Similar to the UMI, the UMZI is actively stabilized by using an auxiliary CW laser of 1553.33 nm, which has the coherence length much larger than the path length difference of the UMZI, to feedback-control the piezo-actuated fiber stretcher. The measurement bases for the time-bin qubits are set by appropriately choosing the phases of the UMZIs ($\phi_A$, $\phi_B$, and $\phi_C$) via the fiber-optic phase modulators. The InGaAs detectors, operated in the triggered mode synchronized to the repetition rate of the pulsed laser, are set at the quantum efficiency of 15% with the dead time of 10 $\mu$s. The detection window is set to 1.5 ns to suppress the possibility of noise clicks.

In our work, to verify the practical feasibility of a quantum network with time-bin entanglement, we have demonstrated the Ekert91 protocol, one of the entangled-photon QKD protocols, with three users. The time synchronization information needs to be distributed as all time-correlated devices belonging to communicating users should be synchronized in performing the communication protocol. The time synchronization information is also needed to operate the detectors in the gated mode. The sync-information is further needed for the key sifting process. Hence, from the practical point of view, the network provider needs to provide the clock signal to all users. The network provider, however, does not need to provide global phase reference signals to users. The time-bin entanglement utilizes a relative phase between successive temporal modes in encoding qubit information. For this reason, a global phase reference is not required in time-bin mode quantum communication.

**TABLE I.** Time-bin two-photon interference data. The 60 km long optical fiber spool does reduce the rate of coincidence counts but hardly affects the two-photon visibilities and the CHSH *S* parameter values. The coincidence rates for Bob–Charlie and Charlie–Alice are smaller due to the slightly higher loss at Charlie's measurement setup.

| | Distance (km) | Coincidence (Hz) | Visibility | CHSH $S$ |
|---|---|---|---|---|
| Alice–Bob | No DSF spool | 22.382 ± 0.346 | 0.940 ± 0.002 | 2.663 ± 0.088 |
| Bob–Charlie | No DSF spool | 15.728 ± 0.119 | 0.948 ± 0.003 | 2.665 ± 0.089 |
| Charlie–Alice | No DSF spool | 16.606 ± 0.133 | 0.942 ± 0.003 | 2.679 ± 0.089 |
| Alice–Bob | 60 | 1.262 ± 0.060 | 0.931 ± 0.008 | 2.627 ± 0.117 |
| Bob–Charlie | 60 | 1.057 ± 0.057 | 0.932 ± 0.009 | 2.648 ± 0.122 |
| Charlie–Alice | 60 | 0.952 ± 0.053 | 0.926 ± 0.010 | 2.615 ± 0.124 |

### B. Simultaneous distribution of time-bin entanglement

The quality of two-qubit time-bin entanglement distributed over 60 km optical fibers can be tested by measuring time-bin two-photon interference (Franson interference)[62–64] or by testing the violation of the CHSH inequality.[65,66] Ideally, for the time-bin entangled state in Eq. (1) with $\phi_p = 0$, i.e., $\frac{1}{\sqrt{2}}(|S\rangle_s|S\rangle_i + |L\rangle_s|L\rangle_i)$, the coincidence probabilities between the detectors at Alice and Bob's setups are calculated to be

$$\begin{aligned} P_{A1,B1} &= P_{A2,B2} = \frac{1}{4}[1+\cos(\phi_A+\phi_B)], \\ P_{A1,B2} &= P_{A2,B1} = \frac{1}{4}[1-\cos(\phi_A+\phi_B)], \end{aligned} \tag{2}$$

where the subscripts are defined in Fig. 1. The coincidence probabilities between the detectors at Bob–Charlie and Charlie–Alice are similarly calculated. In the experiment, the twofold coincidence rate is given by $R_c \propto 1 \pm V\cos(\phi_A + \phi_B)$, where V is the two-photon interference visibility, and it is well known that the condition for violating the CHSH inequality is $V > 1/\sqrt{2} \approx 0.707$.[65]

The experimental data for the time-bin entanglement distribution are summarized in Table I. We first measured the two-photon interference and the CHSH $S$ parameter without the 30 km long dispersion-shifted-fiber (DSF) spools installed. With the observed two-photon interference visibility greater than 0.94, we find that the CHSH inequality is violated for all three pairs of users by at least seven standard deviations. Next, with the 30 km long DSF spools installed, all pairs of users are now fiber-optically linked with 60 km separations. Due to the fiber attenuation of ~0.2 dB/km and additional fiber-optic couplers, the coincidence count rates have become smaller. However, the visibilities of the two-photon interference and the experimental values of the CHSH $S$ parameter have been only minimally affected: we observe the CHSH inequality violation of ~5 standard deviations. An example set of the two-photon interference measurements is shown in Fig. 2. Every user in the quantum network is sharing time-bin entangled qubit pairs with another user via the 60 km long optical fiber spool, and sharing of high-quality entanglement is clearly demonstrated in the data. As mentioned earlier already, Charlie's measurement setup has a slightly lower efficiency, which results in lower coincidence count rates in Figs. 2(b) and 2(c).

### C. Analysis of the system performance

Ultimately, the system performance is limited by the quality of the two-photon interference, i.e., visibility, as functions of external parameters, such as the SPDC generation rate, the channel efficiency, the detector dark counts, and the quality of interferometers. For the time-bin entangled state considered in our work,

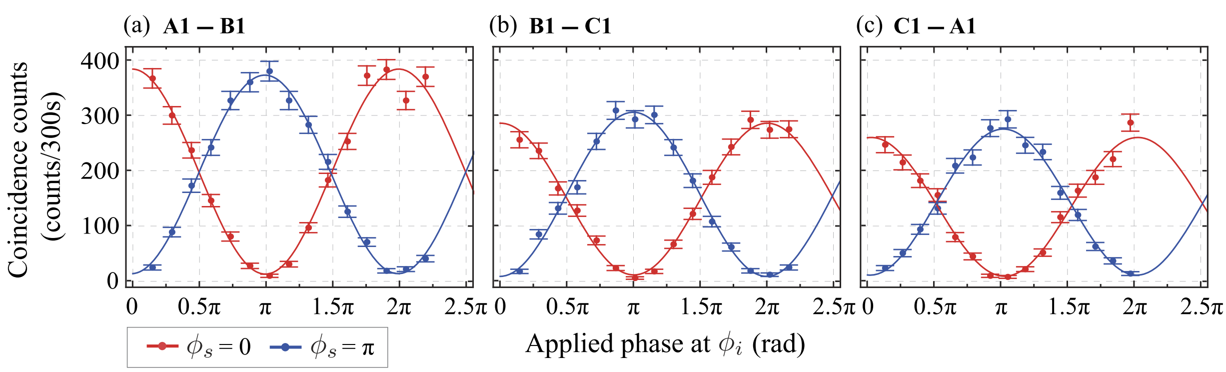


**FIG. 2.** Two-photon interference due to time-bin entangled photons over 60 km optical fibers as functions of the local phase setting in measuring the idler photon $\phi_i$ between (a) Alice and Bob, (b) Bob and Charlie, and (c) Charlie and Alice. The blue (red) solid circles represent the local phase setting in measuring the signal photon at $\phi_s = \pi$ ($\phi_s = 0$). The solid lines are numerical fits to experimental data. The error bars represent one standard deviation assuming Poissonian statistics.

$|\phi\rangle = \frac{1}{\sqrt{2}}(|S\rangle_s|S\rangle_i + |L\rangle_s|L\rangle_i)$, the probability of a coincidence event $P_c$ between the detectors at the two network users (Alice and Bob in Fig. 1, for instance) can be expressed as[67]

$$P_c = \frac{1}{8}\mu\eta_A\eta_B\left(\frac{1}{2} + \frac{1}{2}V_0\cos(\phi_A + \phi_B)\right) + \left(\frac{1}{4}\mu\eta_A + d_A\right)\left(\frac{1}{4}\mu\eta_B + d_B\right), \tag{3}$$

where $\mu$ is the average number of SPDC photon pairs (which can be varied by the pump power), $\eta_A$ ($\eta_B$) is the overall channel efficiency (including fiber transmission efficiency, efficiencies of the various fiber optical components, and the detector efficiency but excluding the DSF spool) measured by Alice (Bob), $V_0$ is the maximum achievable visibility (experimentally limited by the interferometer implementation), $\phi_A$ ($\phi_B$) is the local phase of Alice's (Bob's) UMZI, and $d_A$ ($d_B$) is the dark count probability of the detector belonging to Alice (Bob). Note that the average number of SPDC photon pairs $\mu$ is estimated from the coincidence to accidental ratio (CAR) using the relation $\mu \approx \frac{2}{\text{CAR}-1}$.[67] The coincidence probabilities $P_c$ between the detectors at Bob and Charlie and those of the detectors at Charlie–Alice are similarly calculated. The first term in Eq. (3) refers to the contribution by the entangled photon pair, while the second term represents accidental contributions to the coincidence counts. The accidental coincidence term, of course, limits the two-photon interference visibility V achievable in the experiment as

$$V = \frac{\frac{1}{8}\mu\eta_A\eta_B}{\frac{1}{8}\mu\eta_A\eta_B + 2\left(\frac{1}{4}\mu\eta_A + d_A\right)\left(\frac{1}{4}\mu\eta_B + d_B\right)}V_0 \approx \frac{1}{\mu+1}V_0, \tag{4}$$

where the approximation considers the limiting case $\frac{1}{4}\mu\eta_{A(B)} \gg d_{A(B)}$, i.e., a small dark count contribution to the signal. This approximation is justified, given the experimental condition that the detectors are gated for 1.5 ns time window, giving the dark count probability of $6 \times 10^{-6}$/gate. The two-photon visibility measurements as a function of the average number of SPDC photon pairs $\mu$ with no DSF spools are shown in Fig. 3(a), and the linear decrease in two-photon visibility with the increase in $\mu$ (implemented by increasing the pump power) is observed in accordance with Eq. (4), $V \approx \frac{1}{1+\mu}V_0$. The visibilities gradually decrease due to the increased probabilities of generating multiple SPDC photon pairs with a larger $\mu$.

We can now estimate the two-photon visibility degradation as a function of the channel distances $L_A$ (source to Alice) and $L_B$ (source to Bob) using the known fiber attenuation constant of $\alpha$ = 0.20 dB/km. With the added fiber channel of length $L_A$, the overall channel efficiency for Alice is changed to $\eta_A \to \eta_A 10^{-\alpha\frac{L_A}{10}}$ and similarly for Bob. The two-photon visibility expression in Eq. (4) is then changed to

$$V = \frac{\frac{1}{8}\mu\eta_A\eta_B 10^{-\alpha\frac{L_A+L_B}{10}}}{\frac{1}{8}\mu\eta_A\eta_B 10^{-\alpha\frac{L_A+L_B}{10}} + 2\left(\frac{1}{4}\mu\eta_A 10^{-\alpha\frac{L_A}{10}} + d_A\right)\left(\frac{1}{4}\mu\eta_B 10^{-\alpha\frac{L_B}{10}} + d_B\right)}V_0. \tag{5}$$

The experimental data and the numerical simulation according to Eq. (5) are shown in Fig. 3(b). Here, the channel distances are $L_A = L_B$, which are implemented with a set of 30 km long DSF spools. The observed two-photon visibility data and the numerical simulation results are consistent and show clearly that the unavoidable channel loss of the optical fiber ($\alpha$ = 0.20 dB/km) do contribute to the visibility decrease due to the fact that the environmental noise and the detector dark counts are constant.

## D. Entanglement-based QKD over the quantum network

While the high two-photon interference visibility is a good indicator that entanglement may be distributed, to confirm the successful distribution of time-bin entanglement, $\frac{1}{\sqrt{2}}(|S\rangle_s|S\rangle_i + |L\rangle_s|L\rangle_i$, to pairs of the network users, e.g., Alice–Bob, Bob–Charlie, and Charlie–Alice, it is necessary to measure the CHSH $S$ parameter as the entanglement-based Ekert QKD protocols require the CHSH-Bell inequality violation to test for the presence of eavesdropping.[6,65]

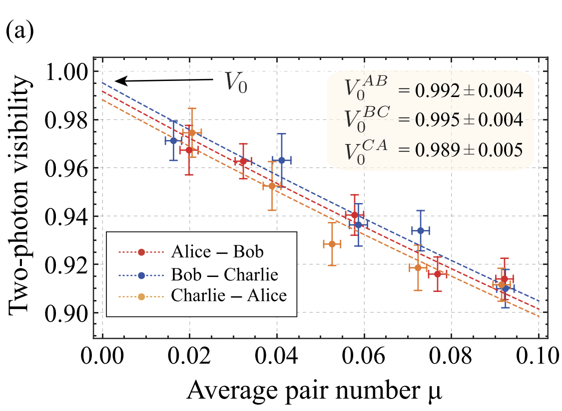


**FIG. 3.** (a) Two-photon visibility as a function of the average number SPDC photon pairs $\mu$ with no DSF spool. A linear decrease in two-photon visibility with the increase in $\mu$ (implemented by increasing the pump power) is observed in accordance with Eq. (4), $V \approx \frac{1}{1+\mu}V_0$ (dotted lines). (b) Two-photon visibility as a function of the channel distance (attenuation at the fiber is $\alpha$ = 0.20 dB/km) at $\mu \approx 0.049$. The visibility degradation (dotted lines) is consistent with Eq. (5). The slightly different tendency for Alice–Bob is due to the fact that Charlie's setup has a lower system efficiency. The overall channel efficiencies are $\eta_A$ = 1.39%, $\eta_B$ = 1.36%, and $\eta_C$ = 1.02%. The data points are slightly displaced horizontally for easier reading.

Ideally, for an initial pure maximally entangled two-qubit state, the CHSH $S$ parameter is related to the two-photon visibility as $S = 2\sqrt{2}V$, with V defined in Eq. (5). Independent verification of the CHSH inequality for the photon pair shared by Alice and Bob, however, requires measuring the CHSH $S$ parameter defined as

$$S = E(\phi_A, \phi_B) + E(\phi'_A, \phi_B) + E(\phi_A, \phi'_B) - E(\phi'_A, \phi'_B),$$

where the experimentally measured correlation $E(\phi_A, \phi_B)$ is defined as

$$E(\phi_A, \phi_B) = \frac{R_{A1,B1} - R_{A1,B2} - R_{A2,B1} + R_{A2,B2}}{R_{A1,B1} + R_{A1,B2} + R_{A2,B1} + R_{A2,B2}}.$$

Here, $R_{A1,B1}$ refers to the measured coincidence count between the detectors $A1$ and $B1$ for Alice's interferometer set at $\phi_A$ and Bob's interferometer set at $\phi_B$, as shown in Fig. 1. Others for different detector combinations are similarly defined. For the maximum violation of the CHSH inequality, we used the measurement bases defined by the local phases $\phi_A$ and $\phi_B$ tabulated in the Appendix. The CHSH inequalities for the photon pair shared by Bob and Charlie and by Charlie and Alice may be evaluated by using similarly defined $S$ parameters.

Depending on the choices of the measurement bases shown in the Appendix, two sets of $S$ measurements (namely, set 1 and set 2) are possible. Both measurement sets show clear violation of the CHSH inequality, as summarized in Table II. The CHSH $S$ parameters for set 1 measurements are shown in Fig. 4(a). The data clearly show the CHSH inequality violation at 60 km of optical fiber separation between the network users. Using the relation between the CHSH $S$ parameter and the two-photon visibility, $S = 2\sqrt{2}V$ with V defined in Eq. (5), it is estimated that the CHSH inequality violation will vanish at 170 km.

In entanglement-photon QKD, the sifted key is established from the joint-detection events by using the measurement basis settings that are not used for the eavesdropping detection, i.e., CHSH $S$ parameter measurements, and the basis settings for the sifted key extraction are shown in the Appendix. The secure key is then extracted from the sifted key by considering a few conditions, and the secure key rate $R_s$ is given by[68,69]

$$R_s \geq qQ_\lambda\{1 - f(\delta_b)H(\delta_b) - H(\delta_p)\}, \tag{6}$$

where $q$ is the basis reconciliation factor (1/4 for the Ekert protocol), $Q_\lambda$ is the overall gain or the probability of a joint-detection event given a pump pulse ($\mu = 2\lambda$ is the average number of the SPDC photon pair),[69] $\delta_b$ is the bit error rate, $\delta_p$ is the phase error rate, $f(\delta_b)$ is the error correction efficiency, and $H(x) = -x\log_2(x) - (1-x)\log_2(1-x)$ is the binary entropy function. The secure key rate $R_s$ in Eq. (6) is derived for coherent attacks, so it provides an optimal security guarantee and is valid for the asymptotic limit of an infinitely long key string.[68,69] In this work, we assume $\delta_b = \delta_p$ as the measurement basis is symmetric, and hence, we have $\delta_b = \delta_p = \mathcal{E}_\lambda$, where $\mathcal{E}_\lambda = (1-V)/2$ is the quantum bit error rate (QBER) for the

**TABLE II.** Experimental pairwise QKD in a wavelength-multiplexed fiber network.

| | Distance | QBER (%) | Sifted key rate (bits/s) | Secure key rate (bits/s) | S parameter (set 1/set 2) |
|---|---|---|---|---|---|
| Alice–Bob | No DSF spool | 2.76 ± 0.11 | 8.087 ± 0.050 | 5.137 ± 0.093 | 2.680 ± 0.030/2.633 ± 0.029 |
| Bob–Charlie | No DSF spool | 3.21 ± 0.14 | 5.055 ± 0.040 | 2.984 ± 0.075 | 2.579 ± 0.038/2.688 ± 0.038 |
| Charlie–Alice | No DSF spool | 3.14 ± 0.13 | 5.629 ± 0.042 | 3.364 ± 0.079 | 2.737 ± 0.036/2.586 ± 0.036 |
| Alice–Bob | 60 km | 3.58 ± 0.20 | 0.467 ± 0.005 | 0.259 ± 0.009 | 2.618 ± 0.051/2.607 ± 0.051 |
| Bob–Charlie | 60 km | 3.73 ± 0.25 | 0.327 ± 0.004 | 0.177 ± 0.008 | 2.598 ± 0.060/2.639 ± 0.060 |
| Charlie–Alice | 60 km | 3.81 ± 0.26 | 0.317 ± 0.004 | 0.169 ± 0.008 | 2.716 ± 0.062/2.615 ± 0.063 |

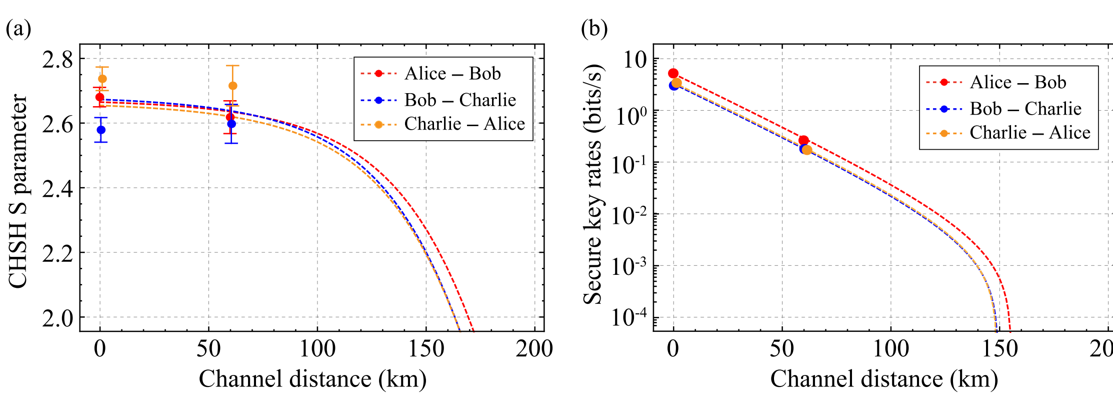


**FIG. 4.** (a) Measured CHSH $S$ parameters for the distance of zero and 60 km long optical fiber channels between the users (using the measurement basis set 1 in the Appendix). The CHSH inequality violation vanishes ($S = 2$) roughly at 170 km. The dotted lines are calculated from Eq. (5) using $S = 2\sqrt{2}V$. (b) Secure key generation rates for the Ekert protocol. Roughly at 150 km of optical fiber transmission, the secure key generation rate $R_s$ is expected to drop to zero. The dotted lines are due to Eq. (6). All the measurements are done with $\mu \approx 0.049$. The error bars represent one standard deviation, and the data points are slightly displaced for easier reading.

system and is evaluated from the two-photon interference visibility V. The secure key rate $R_s$ can be estimated from the experimental sifted key rate using Eq. (6) assuming $f(\delta_b) = 1$ (the Shannon limit), and the results are shown in Fig. 4(b) as well as summarized in Table II. The secure key rates are expected to drop to zero at around 150 km, which corresponds to $R_s = 0$ at $\mathcal{E}_\lambda \approx 11\%$.

Using super-conducting nanowire single-photon detectors (SNSPDs), instead of InGaAs single-photon detectors, would significantly improve the QKD performance due to low dark counts and higher quantum efficiency, and the improvement can be estimated by starting from Eq. (5). For SNSPDs, the quantum efficiency is at least five times better than those of InGaAs single-photon detectors and the dark count probability is about 100 times lower. Then, the relevant parameters are $\mu \approx 0.049$, $\eta_A = 5 \times 1.39\%$, $\eta_B = 5 \times 1.36\%$, $\eta_C = 5 \times 1.02\%$, and the dark count probability of $6 \times 10^{-8}$/gate which would result the maximum achievable visibilities $V_0^{AB} = 0.992$, $V_0^{BC} = 0.995$, and $V_0^{CA} = 0.989$. Based on the above parameters, the secure key rates $R_s$ can be evaluated. The simulation results show that if SNSPDs were used instead of InGaAs detectors, there would be significant improvement in the maximum channel distance for quantum key distribution: up to 420 km compared to 150 km for the case of InGaAs detectors.

### E. Discussion

While our setup is, in principle, field-deployable, it is important to consider a few technical problems in actually implementing our setup in a real-world environment.[70–72] First, synchronization among network nodes is one of the main issues. All electronic and electro-optic devices, e.g., detectors and phase modulators, must be synchronized to a reference clock for accurate qubit encoding and photon counting. In this work, we rely on electronic synchronization pulses from the main laser to synchronize all three users in the network. Second, the environmental change, including weather status, would directly affect the temperature fluctuation, birefringence, optical path length, and transmission loss in optic-fiber channels, which, in turn, cause unavoidable difficulties in performing field experiments. Moreover, these degradations accumulate with distance. Interestingly, the random birefringence effects induced in deployed fibers do not affect the time-bin entanglement because for a time-bin entanglement, quantum information is encoded in the relative phase between successive temporal modes. For this reason, the phase stability of the interferometer is a significant issue in time-bin based communication and needs to be well maintained using a feedback system, the details of which are well-described in Sec. II A. While time-bin entanglement does not degrade due to polarization effects in fiber transmission, environmental effects on the phase modulator's optic axes could still affect the quality of time-bin entanglement, albeit small it may be. To fully prevent this effect, polarization compensation needs to be actively performed if the system is deployed in an outdoor environment.[73]

The optical noise in the fiber channel is also a major concern. The presence of channel noise is unavoidable because the noise is generated from stray light and the cross-talk of co-propagating classical signals. Then, a perfectly prepared entangled state on the noisy fiber channel could quickly degrade to a low-fidelity mixed state, precluding quantum communication in the end. Given the importance of high-quality entanglement distribution, effective noise suppression approaches have been performed, including passive strategies (e.g., adopting low-noise detectors) or the application of noise-resistant quantum communication protocol.[74]

## III. CONCLUSION

We have reported an experimental demonstration of a quantum communication system capable of distributing time-bin entangled qubit pairs over a wavelength-multiplexed fiber network. Owing to the use of the broadband nature of type-0 SPDC process and WDM components, all network users are simultaneously ready for quantum communication with another user within the network. In addition, the use of time-bin entangled photonic qubits offers robustness for long-distance transmission compared with the case of polarization-entangled photonic qubits which are susceptible to various polarization-mode dispersion effects in the fibers. Moreover, the temporal degree of freedom is intrinsically easier for encoding high-dimensional quantum states, qudits, thus allowing us to more easily utilize qudit entanglement for quantum communication experiments.

The experimental demonstration reported here may be easily expanded, with minimal efforts, to include multiple network users by utilizing additional WDM components. This is made possible because only a single entangled-photon source, which distributes a pair of time-bin entangled qubits to any two members of the quantum network, is required and, through the use of the wavelength-division demultiplexing/multiplexing technology, all the network members are simultaneously ready for quantum communication. The fact that each network member does not have to be equipped with its own entangled-photon source (only the network provider needs to be equipped with the entangled-photon source) greatly reduces the complexity and the cost of the network setup.

The proposed quantum communication network setup, thus, is quite field-deployable in the sense that all the components used in the experiments are commercially and readily available.

## ACKNOWLEDGMENTS

This work was supported, in part, by the National Research Foundation of Korea (Grant No. 2019R1A2C3004812), the Affiliated Institute of ETRI (Grant No. 2019-110), and the ITRC support program (Grant No. IITP-2021-2020-0-01606).

## AUTHOR DECLARATIONS

### Conflict of Interest

The authors have no conflicts to disclose.

## DATA AVAILABILITY

The data that support the findings of this study are available from the corresponding author upon reasonable request.

## APPENDIX: MEASUREMENT BASES

For QKD with time-bin entangled qubits, it is necessary to choose proper local phases at the end users' interferometers to

TABLE III. The local phase settings for Alice and Bob's interferometers, UMZIs shown in Fig. 1, to determine the measurement bases.

| | $\phi_A = 0°$ | $\phi_A = 45°$ | $\phi_A = 90°$ | $\phi_A = 135°$ |
|---|---|---|---|---|
| $\phi_B = 45°$ | CHSH inequality (set 1) | Not used | CHSH inequality (set 1) | Secret key |
| $\phi_B = 90°$ | Not used | CHSH inequality (set 2) | Secret key | CHSH inequality (set 2) |
| $\phi_B = 135°$ | CHSH inequality (set 1) | Secret key | CHSH inequality (set 1) | Not used |
| $\phi_B = 180°$ | Secret key | CHSH inequality (set 2) | Not used | CHSH inequality (set 2) |

properly set the measurement bases. For Alice and Bob's interferometers (UMI in Fig. 1), $\phi_A$ and $\phi_B$ need to be properly chosen for the eavesdropping detection via CHSH $S$ parameter measurement and for key distribution, as shown in Table III. For the CHSH inequality measurement, two different measurement bases are available, referred to as set 1 and set 2. The phase settings for Bob–Charlie and Charlie–Alice are similarly defined.

## REFERENCES


[1] C. H. Bennett, G. Brassard, C. Crépeau, R. Jozsa, A. Peres, and W. K. Wootters, "Teleporting an unknown quantum state via dual classical and Einstein-Podolsky-Rosen channels," Phys. Rev. Lett. **70**(13), 1895–1899 (1993).

[2] D. Bouwmeester, J.-W. Pan, K. Mattle, M. Eibl, H. Weinfurter, and A. Zeilinger, "Experimental quantum teleportation," Nature **390**(6660), 575–579 (1997).

[3] D. Boschi, S. Branca, F. De Martini, L. Hardy, and S. Popescu, "Experimental realization of teleporting an unknown pure quantum state via dual classical and Einstein-Podolsky-Rosen channels," Phys. Rev. Lett. **80**(6), 1121–1125 (1998).

[4] Y.-H. Kim, S. P. Kulik, and Y. Shih, "Quantum teleportation of a polarization state with a complete Bell state measurement," Phys. Rev. Lett. **86**(7), 1370–1373 (2001).

[5] X.-S. Ma, T. Herbst, T. Scheidl, D. Wang, S. Kropatschek, W. Naylor, B. Wittmann, A. Mech, J. Kofler, E. Anisimova, V. Makarov, T. Jennewein, R. Ursin, and A. Zeilinger, "Quantum teleportation over 143 kilometres using active feed-forward," Nature **489**(7415), 269–273 (2012).

[6] A. K. Ekert, "Quantum cryptography based on Bell's theorem," Phys. Rev. Lett. **67**(6), 661–663 (1991).

[7] R. Ursin, F. Tiefenbacher, T. Schmitt-Manderbach, H. Weier, T. Scheidl, M. Lindenthal, B. Blauensteiner, T. Jennewein, J. Perdigues, P. Trojek, B. Ömer, M. Fürst, M. Meyenburg, J. Rarity, Z. Sodnik, C. Barbieri, H. Weinfurter, and A. Zeilinger, "Entanglement-based quantum communication over 144 km," Nat. Phys. **3**(7), 481–486 (2007).

[8] F. Xu, X. Ma, Q. Zhang, H.-K. Lo, and J.-W. Pan, "Secure quantum key distribution with realistic devices," Rev. Mod. Phys. **92**(2), 025002 (2020).

[9] J. Yin, Y.-H. Li, S.-K. Liao, M. Yang, Y. Cao, L. Zhang, J.-G. Ren, W.-Q. Cai, W.-Y. Liu, S.-L. Li, R. Shu, Y.-M. Huang, L. Deng, L. Li, Q. Zhang, N.-L. Liu, Y.-A. Chen, C.-Y. Lu, X.-B. Wang, F. Xu, J.-Y. Wang, C.-Z. Peng, A. K. Ekert, and J.-W. Pan, "Entanglement-based secure quantum cryptography over 1,120 kilometres," Nature **582**(7813), 501–505 (2020).

[10] C. H. Bennett and S. J. Wiesner, "Communication via one- and two-particle operators on Einstein-Podolsky-Rosen states," Phys. Rev. Lett. **69**(20), 2881–2884 (1992).

[11] J. T. Barreiro, T.-C. Wei, and P. G. Kwiat, "Beating the channel capacity limit for linear photonic superdense coding," Nat. Phys. **4**(4), 282–286 (2008).

[12] B. P. Williams, R. J. Sadlier, and T. S. Humble, "Superdense coding over optical fiber links with complete Bell-state measurements," Phys. Rev. Lett. **118**(5), 050501 (2017).

[13] M. Hillery, V. Bužek, and A. Berthiaume, "Quantum secret sharing," Phys. Rev. A **59**(3), 1829 (1999).

[14] W. Tittel, H. Zbinden, and N. Gisin, "Experimental demonstration of quantum secret sharing," Phys. Rev. A **63**(4), 042301 (2001).

[15] S. Gaertner, C. Kurtsiefer, M. Bourennane, and H. Weinfurter, "Experimental demonstration of four-party quantum secret sharing," Phys. Rev. Lett. **98**(2), 020503 (2007).

[16] S.-K. Liao, W.-Q. Cai, W.-Y. Liu, L. Zhang, Y. Li, J.-G. Ren, J. Yin, Q. Shen, Y. Cao, Z.-P. Li, F.-Z. Li, X.-W. Chen, L.-H. Sun, J.-J. Jia, J.-C. Wu, X.-J. Jiang, J.-F. Wang, Y.-M. Huang, Q. Wang, Y.-L. Zhou, L. Deng, T. Xi, L. Ma, T. Hu, Q. Zhang, Y.-A. Chen, N.-L. Liu, X.-B. Wang, Z.-C. Zhu, C.-Y. Lu, R. Shu, C.-Z. Peng, J.-Y. Wang, and J.-W. Pan, "Satellite-to-ground quantum key distribution," Nature **549**(7670), 43–47 (2017).

[17] S.-K. Liao, H.-L. Yong, C. Liu, G.-L. Shentu, D.-D. Li, J. Lin, H. Dai, S.-Q. Zhao, B. Li, J.-Y. Guan, W. Chen, Y.-H. Gong, Y. Li, Z.-H. Lin, G.-S. Pan, J. S. Pelc, M. M. Fejer, W.-Z. Zhang, W.-Y. Liu, J. Yin, J.-G. Ren, X.-B. Wang, Q. Zhang, C.-Z. Peng, and J.-W. Pan, "Long-distance free-space quantum key distribution in daylight towards inter-satellite communication," Nat. Photonics **11**(8), 509–513 (2017).

[18] T. Inagaki, N. Matsuda, O. Tadanaga, M. Asobe, and H. Takesue, "Entanglement distribution over 300 km of fiber," Opt. Express **21**(20), 23241–23249 (2013).

[19] H.-L. Yin, T.-Y. Chen, Z.-W. Yu, H. Liu, L.-X. You, Y.-H. Zhou, S.-J. Chen, Y. Mao, M.-Q. Huang, W.-J. Zhang, H. Chen, M. J. Li, D. Nolan, F. Zhou, X. Jiang, Z. Wang, Q. Zhang, X.-B. Wang, and J.-W. Pan, "Measurement-device-independent quantum key distribution over a 404 km optical fiber," Phys. Rev. Lett. **117**(19), 190501 (2016).

[20] H.-J. Briegel, W. Dür, J. I. Cirac, and P. Zoller, "Quantum repeaters: The role of imperfect local operations in quantum communication," Phys. Rev. Lett. **81**(26), 5932–5935 (1998).

[21] L.-M. Duan, M. D. Lukin, J. I. Cirac, and P. Zoller, "Long-distance quantum communication with atomic ensembles and linear optics," Nature **414**(6862), 413–418 (2001).

[22] N. Sangouard, C. Simon, H. de Riedmatten, and N. Gisin, "Quantum repeaters based on atomic ensembles and linear optics," Rev. Mod. Phys. **83**(1), 33 (2011).

[23] K. S. Choi, H. Deng, J. Laurat, and H. J. Kimble, "Mapping photonic entanglement into and out of a quantum memory," Nature **452**(7183), 67–71 (2008).

[24] A. I. Lvovsky, B. C. Sanders, and W. Tittel, "Optical quantum memory," Nat. Photonics **3**(12), 706–714 (2009).

[25] Y.-W. Cho and Y.-H. Kim, "Atomic vapor quantum memory for a photonic polarization qubit," Opt. Express **18**(25), 25786–25793 (2010).

[26] X.-H. Bao, A. Reingruber, P. Dietrich, J. Rui, A. Dück, T. Strassel, L. Li, N.-L. Liu, B. Zhao, and J.-W. Pan, "Efficient and long-lived quantum memory with cold atoms inside a ring cavity," Nat. Phys. **8**(7), 517–521 (2012).

[27] K.-K. Park, Y.-W. Cho, Y.-T. Chough, and Y.-H. Kim, "Experimental demonstration of quantum stationary light pulses in an atomic ensemble," Phys. Rev. X **8**(2), 021016 (2018).

[28] M. Koashi and M. Ueda, "Reversing measurement and probabilistic quantum error correction," Phys. Rev. Lett. **82**(12), 2598–2601 (1999).

[29] J.-C. Lee, Y.-C. Jeong, Y.-S. Kim, and Y.-H. Kim, "Experimental demonstration of decoherence suppression via quantum measurement reversal," Opt. Express **19**(17), 16309–16316 (2011).

[30] Y.-S. Kim, J.-C. Lee, O. Kwon, and Y.-H. Kim, "Protecting entanglement from decoherence using weak measurement and quantum measurement reversal," Nat. Phys. **8**(2), 117–120 (2012).

[31]J. C. Lee, H. T. Lim, K. H. Hong, Y. C. Jeong, M. S. Kim, and Y. H. Kim, "Experimental demonstration of delayed-choice decoherence suppression," Nat. Commun. **5**(1), 4522 (2014).
[32]A. Mair, A. Vaziri, G. Weihs, and A. Zeilinger, "Entanglement of the orbital angular momentum states of photons," Nature **412**(6844), 313–316 (2001).
[33]A. C. Dada, J. Leach, G. S. Buller, M. J. Padgett, and E. Andersson, "Experimental high-dimensional two-photon entanglement and violations of generalized Bell inequalities," Nat. Phys. **7**(9), 677–680 (2011).
[34]J.-C. Lee, K.-K. Park, T.-M. Zhao, and Y.-H. Kim, "Einstein-Podolsky-Rosen entanglement of narrow-band photons from cold atoms," Phys. Rev. Lett. **117**(25), 250501 (2016).
[35]M. Erhard, M. Krenn, and A. Zeilinger, "Advances in high-dimensional quantum entanglement," Nat. Rev. Phys. **2**(7), 365–381 (2020).
[36]J. T. Barreiro, N. K. Langford, N. A. Peters, and P. G. Kwiat, "Generation of hyperentangled photon pairs," Phys. Rev. Lett. **95**(26), 260501 (2005).
[37]T. M. Graham, H. J. Bernstein, T.-C. Wei, M. Junge, and P. G. Kwiat, "Superdense teleportation using hyperentangled photons," Nat. Commun. **6**(1), 7185 (2015).
[38]T.-M. Zhao, Y. S. Ihn, and Y.-H. Kim, "Direct generation of narrow-band hyperentangled photons," Phys. Rev. Lett. **122**(12), 123607 (2019).
[39]C. Wang, C.-H. Lee, Y. Kim, and Y.-H. Kim, "Generation of hyper-entangled photons in a hot atomic vapor," Opt. Lett. **45**(7), 1802–1805 (2020).
[40]M. Peev, C. Pacher, R. Alléaume, C. Barreiro, J. Bouda, W. Boxleitner, T. Debuisschert, E. Diamanti, M. Dianati, J. F. Dynes, S. Fasel, S. Fossier, M. Fürst, J.-D. Gautier, O. Gay, N. Gisin, P. Grangier, A. Happe, Y. Hasani, M. Hentschel, H. Hübel, G. Humer, T. Länger, M. Legré, R. Lieger, J. Lodewyck, T. Lorünser, N. Lütkenhaus, A. Marhold, T. Matyus, O. Maurhart, L. Monat, S. Nauerth, J.-B. Page, A. Poppe, E. Querasser, G. Ribordy, S. Robyr, L. Salvail, A. W. Sharpe, A. J. Shields, D. Stucki, M. Suda, C. Tamas, T. Themel, R. T. Thew, Y. Thoma, A. Treiber, P. Trinkler, R. Tualle-Brouri, F. Vannel, N. Walenta, H. Weier, H. Weinfurter, I. Wimberger, Z. L. Yuan, H. Zbinden, and A. Zeilinger, "The SECOQC quantum key distribution network in Vienna," New J. Phys. **11**(7), 075001 (2009).
[41]M. Sasaki, M. Fujiwara, H. Ishizuka, W. Klaus, K. Wakui, M. Takeoka, S. Miki, T. Yamashita, Z. Wang, A. Tanaka, K. Yoshino, Y. Nambu, S. Takahashi, A. Tajima, A. Tomita, T. Domeki, T. Hasegawa, Y. Sakai, H. Kobayashi, T. Asai, K. Shimizu, T. Tokura, T. Tsurumaru, M. Matsui, T. Honjo, K. Tamaki, H. Takesue, Y. Tokura, J. F. Dynes, A. R. Dixon, A. W. Sharpe, Z. L. Yuan, A. J. Shields, S. Uchikoga, M. Legré, S. Robyr, P. Trinkler, L. Monat, J.-B. Page, G. Ribordy, A. Poppe, A. Allacher, O. Maurhart, T. Länger, M. Peev, and A. Zeilinger, "Field test of quantum key distribution in the Tokyo QKD network," Opt. Express **19**(11), 10387–10409 (2011).
[42]D. Stucki, M. Legré, F. Buntschu, B. Clausen, N. Felber, N. Gisin, L. Henzen, P. Junod, G. Litzistorf, P. Monbaron, L. Monat, J.-B. Page, D. Perroud, G. Ribordy, A. Rochas, S. Robyr, J. Tavares, R. Thew, P. Trinkler, S. Ventura, R. Voirol, N. Walenta, and H. Zbinden, "Long-term performance of the SwissQuantum quantum key distribution network in a field environment," New J. Phys. **13**(12), 123001 (2011).
[43]T.-Y. Chen, X. Jiang, S.-B. Tang, L. Zhou, X. Yuan, H. Zhou, J. Wang, Y. Liu, L.-K. Chen, W.-Y. Liu, H.-F. Zhang, K. Cui, H. Liang, X.-G. Li, Y. Mao, L.-J. Wang, S.-B. Feng, Q. Chen, Q. Zhang, L. Li, N.-L. Liu, C.-Z. Peng, X. Ma, Y. Zhao, and J.-W. Pan, "Implementation of a 46-node quantum metropolitan area network," npj Quantum Inf. **7**, 134 (2021).
[44]P. Toliver, R. J. Runser, T. E. Chapuran, J. L. Jackel, T. C. Banwell, M. S. Goodman, R. J. Hughes, C. G. Peterson, D. Derkacs, J. E. Nordholt, L. Mercer, S. McNown, A. Goldman, and J. Blake, "Experimental investigation of quantum key distribution through transparent optical switch Elements," IEEE Photonics Technol. Lett. **15**(11), 1669–1671 (2003).
[45]I. Herbauts, B. Blauensteiner, A. Poppe, T. Jennewein, and H. Hübel, "Demonstration of active routing of entanglement in a multi-user network," Opt. Express **21**(23), 29013–29024 (2013).
[46]X.-Y. Chang, D.-L. Deng, X.-X. Yuan, P.-Y. Hou, Y.-Y. Huang, and L.-M. Duan, "Experimental realization of an entanglement access network and secure multi-party computation," Sci. Rep. **6**, 29453 (2016).
[47]C. Kupchak, J. Erskine, D. England, and B. Sussman, "Terahertz-bandwidth switching of heralded single photons," Opt. Lett. **44**(6), 1427–1430 (2019).
[48]J. Trapateau, J. Ghalbouni, A. Orieux, E. Diamanti, and I. Zaquine, "Multi-user distribution of polarization entangled photon pairs," J. Appl. Phys. **118**(14), 143106 (2015).
[49]D. Aktas, B. Fedrici, F. Kaiser, T. Lunghi, L. Labonté, and S. Tanzilli, "Entanglement distribution over 150 km in wavelength division multiplexed channels for quantum cryptography," Laser Photonics Rev. **10**(3), 451–457 (2016).
[50]Y.-H. Li, Z.-Y. Zhou, Z.-H. Xu, L.-X. Xu, B.-S. Shi, and G.-C. Guo, "Multiplexed entangled photon-pair sources for all-fiber quantum networks," Phys. Rev. A **94**(4), 043810 (2016).
[51]S. Wengerowsky, S. K. Joshi, F. Steinlechner, H. Hübel, and R. Ursin, "An entanglement-based wavelength-multiplexed quantum communication network," Nature **564**(7735), 225–258 (2018).
[52]S. K. Joshi, D. Aktas, S. Wengerowsky, M. Lončarić, S. P. Neumann, B. Liu, T. Scheidl, G. C. Lorenzo, Ź. Samec, L. Kling, A. Qiu, M. Razavi, M. Stipčević, J. G. Rarity, and R. Ursin, "A trusted node-free eight-user metropolitan quantum communication network," Sci. Adv. **6**(36), eaba0959 (2020).
[53]N. B. Lingaraju, H.-H. Lu, S. Seshadri, D. E. Leaird, A. M. Weiner, and J. M. Lukens, "Adaptive bandwidth management for entanglement distribution in quantum networks," Optica **8**(3), 329–332 (2021).
[54]F. Appas, F. Baboux, M. I. Amanti, A. Lemaítre, F. Boitier, E. Diamanti, and S. Ducci, "Flexible entanglement-distribution network with an AlGaAs chip for secure communications," npj Quantum Inf. **7**, 118 (2021).
[55]M. Alshowkan, B. P. Williams, P. G. Evans, N. S. V. Rao, E. M. Simmerman, H.-H. Lu, N. B. Lingaraju, A. M. Weiner, C. E. Marvinney, Y.-Y. Pai, B. J. Lawrie, N. A. Peters, and J. M. Lukens, "Reconfigurable quantum local area network over deployed fiber," PRX Quantum **2**(4), 040304 (2021).
[56]W. Y. Hwang, "Quantum key distribution with high loss: Toward global secure communication," Phys. Rev. Lett. **91**(5), 057901 (2003).
[57]Y. Zhao, B. Qi, X. Ma, Hk. Lo, and L. Qian, "Experimental quantum key distribution with decoy states," Phys. Rev. Lett. **96**(7), 070502 (2006).
[58]M. Lucamarini, Z. L. Yuan, J. F. Dynes, and A. J. Shields, "Overcoming the rate–distance limit of quantum key distribution without quantum repeaters," Nature **557**(7705), 400–403 (2018).
[59]C. Clivati, A. Meda, S. Donadello, S. Virzì, M. Genovese, F. Levi, A. Mura, M. Pittaluga, Z. L. Yuan, A. J. Shields, M. Lucamarini, I. P. Degiovanni, and D. Calonico, "Coherent phase transfer for real-world twin-field quantum key distribution," arXiv:2012.15199 (2020).
[60]J.-P. Chen, C. Zhang, Y. Liu, C. Jiang, W.-J. Zhang, Z.-Y. Han, S.-Z. Ma, X.-L. Hu, Y.-H. Li, H. Liu, F. Zhou, H.-F. Jiang, T.-Y. Chen, H. Li, L.-X. You, Z. Wang, X.-B. Wang, Q. Zhang, and J.-W. Pan, "Twin-field quantum key distribution over a 511 km optical fibre linking two distant metropolitan areas," Nat. Photonics **15**, 570–575 (2021).
[61]H. Liu, C. Jiang, H.-T. Zhu, M. Zou, Z.-W. Yu, X.-L. Hu, H. Xu, S. Ma, Z. Han, J.-P. Chen, Y. Dai, S.-B. Tang, W. Zhang, H. Li, L. You, Z. Wang, Y. Hua, H. Hu, H. Zhang, F. Zhou, Q. Zhang, X.-B. Wang, T.-Y. Chen, and J.-W. Pan, "Field test of twin-field quantum key distribution through sending-or-not-sending over 428 km," Phys. Rev. Lett. **126**(25), 250502 (2021).
[62]I. Marcikic, H. de Riedmatten, W. Tittel, H. Zbinden, M. Legré, and N. Gisin, "Distribution of time-bin entangled qubits over 50 km of optical fiber," Phys. Rev. Lett. **93**(18), 180502 (2004).
[63]J. M. Donohue, M. Agnew, J. Lavoie, and K. J. Resch, "Coherent ultrafast measurement of time-bin encoded photons," Phys. Rev. Lett. **111**(15), 153602 (2013).
[64]O. Kwon, K.-K. Park, Y.-S. Ra, Y.-S. Kim, and Y.-H. Kim, "Time-bin entangled photon pairs from spontaneous parametric down-conversion pumped by a cw multi-mode diode laser," Opt. Express **21**(21), 25492–25500 (2013).
[65]J. F. Clauser, M. A. Horne, A. Shimony, and R. A. Holt, "Proposed experiment to test local hidden-variable theories," Phys. Rev. Lett. **23**(15), 880–884 (1969).
[66]N. Brunner, D. Cavalcanti, S. Pironio, V. Scarani, and S. Wehner, "Bell nonlocality," Rev. Mod. Phys. **86**(2), 419–478 (2014).
[67]H. Takesue and K. Shimizu, "Effects of multiple pairs on visibility measurements of entangled photons generated by spontaneous parametric processes," Opt. Commun. **283**(2), 276–287 (2010).
[68]M. Koashi and J. Preskill, "Secure quantum key distribution with an uncharacterized source," Phys. Rev. Lett. **90**(5), 057902 (2003).

[69]X. Ma, C.-H. F. Fung, and H.-K. Lo, "Quantum key distribution with entangled photon sources," Phys. Rev. A **76**(1), 012307 (2007).
[70]S. Wang, W. Chen, Z.-Q. Yin, H.-W. Li, D.-Y. He, Y.-H. Li, Z. Zhou, X.-T. Song, F.-Y. Li, D. Wang, H. Chen, Y.-G. Han, J.-Z. Huang, J.-F. Guo, P.-L. Hao, M. Li, C.-M. Zhang, D. Liu, W.-Y. Liang, C.-H. Miao, P. Wu, G.-C. Guo, and Z.-F. Han, "Field and long-term demonstration of a wide area quantum key distribution network," Opt. Express **22**(18), 21739–21756 (2014).
[71]E. Diamanti, H.-K. Lo, B. Qi, and Z. Yuan, "Practical challenges in quantum key distribution," npj Quantum Inf. **2**, 16025 (2016).
[72]Q. Zhang, F. Xu, Y.-A. Chen, C.-Z. Peng, and J.-W. Pan, "Large scale quantum key distribution: Challenges and solutions," Opt. Express **26**(18), 24260–24273 (2018).
[73]G. B. Xavier, N. Walenta, G. Vilela de Faria, G. P. Temporão, N. Gisin, H. Zbinden, and J. P. von der Weid, "Experimental polarization encoded quantum key distribution over optical fibres with real-time continuous birefringence compensation," New J. Phys. **11**(4), 045015 (2009).
[74]J.-H. Kim, Y. Kim, D.-G. Im, C.-H. Lee, J.-W. Chae, G. Scarcelli, and Y.-H. Kim, "Noise-resistant quantum communications using hyperentanglement," Optica **8**(12), 1524–1531 (2021).